ACADEMIC
PRESS

Quantitative characterization of biomolecular assemblies and interactions using atomic force microscopy

Yong Yang,[a] Hong Wang,[a,b] and Dorothy A. Erie[a,b,*]

[a] *Department of Chemistry, University of North Carolina at Chapel Hill at Chapel Hill, Chapel Hill, NC 27599, USA*
[b] *Curriculum in Materials Science, University of North Carolina at Chapel Hill, Chapel Hill, NC 27599, USA*

Abstract

Atomic force microscopy (AFM) has been applied in many biological investigations in the past 15 years. This review focuses on the application of AFM for quantitatively characterizing the structural and thermodynamic properties of protein–protein and protein–nucleic acid complexes. AFM can be used to determine the stoichiometries and association constants of multiprotein assemblies and to quantify changes in conformations of proteins and protein–nucleic acid complexes. In addition, AFM in solution permits the observation of the dynamic properties of biomolecular complexes and the measurement of intermolecular forces between biomolecules. Recent advances in cryogenic AFM, AFM on two-dimensional crystals, carbon nanotube probes, solution imaging, high-speed AFM, and manipulation capabilities enhance these applications by improving AFM resolution and the dynamic and operative capabilities of the AFM. These developments make AFM a powerful tool for investigating the biomolecular assemblies and interactions that govern gene regulation.
© 2003 Elsevier Science (USA). All rights reserved.

Keywords: Atomic force microscopy (AFM); Force microscopy; DNA–protein interactions; Protein–protein interactions; Single-molecule techniques; Solution imaging; Volume analysis; Gene regulation; Stoichiometry; Association constants

1. Introduction

Atomic force microscopy (AFM), which was invented in 1986, expanded the application of scanning tunneling microscopy to nonconductive, soft, and live biological samples [1–3]. AFM has several capabilities including characterizing topographic details of surfaces from the submolecular level to the cellular level [4], monitoring the dynamic processes of single molecules in physiologically relevant solutions [5], and measuring the forces between interacting molecules [6]. AFM is a powerful tool for characterizing the structural properties of macromolecular complexes both in air and under near-physiological conditions. In addition, modified AFMs can be used to manipulate single molecules. In the past 15 years, the application of AFM has spread to many areas of biological sciences including studies of DNA [7,8], RNA [9–12], proteins [13,14], lipids [15,16], carbohydrates [17–19], biomolecular complexes [20–22], organelles [23,24] and cells [25,26]. This article focuses on the use of AFM for quantifying biomolecular assemblies and interactions and on recent advances that enhance these applications.

2. Use of AFM

2.1. Principles of AFM

The principle of AFM varies with the different modes of AFM operation, such as contact mode, oscillating mode, and force mode. In the contact mode, the AFM cantilever is deflected by the sample surface. A fixed deflection is maintained during an $X–Y$ dimensional scan by adjusting the Z position of the piezo (Fig. 1A). The AFM image is generated by plotting the Z movement of piezo as a function of the $X–Y$ position. In the
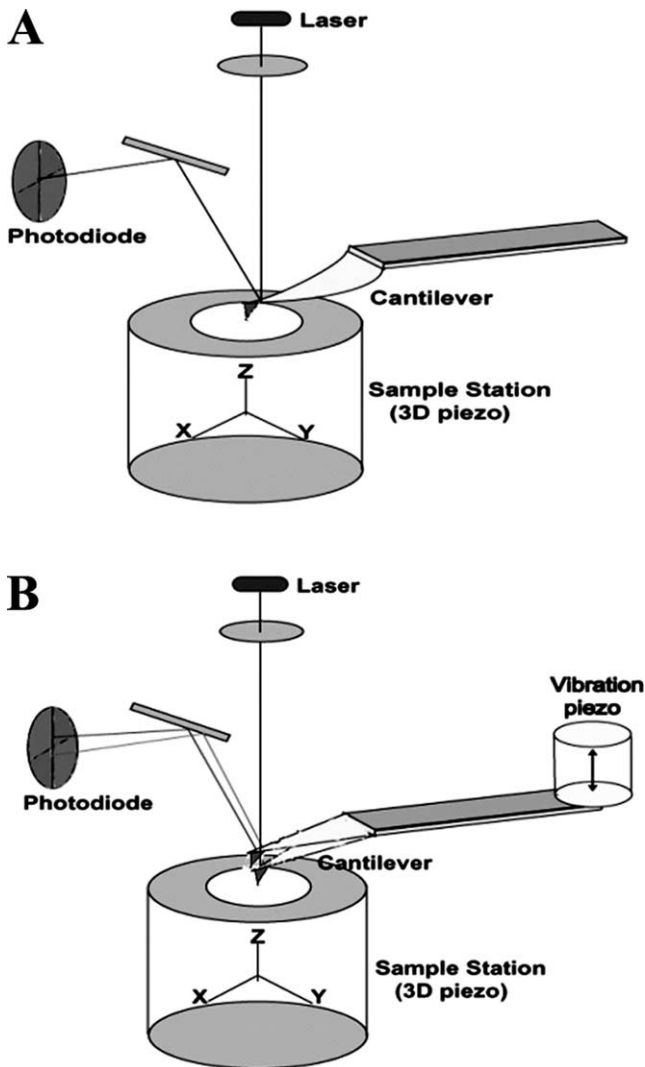

A

B

Fig. 1. Schematics of AFM in the contact mode (A) and the oscillating mode (B).

oscillating mode, the cantilever is oscillated by a vibration piezo. The sample surface is brought into contact with the oscillating cantilever such that it clips the amplitude of oscillation (Fig. 1B). The amplitude of this oscillation, which is monitored by the laser projected on the photodiode, is maintained constant during the scan by adjusting the Z position of the piezo using a feedback loop. The AFM image in the oscillating mode is generated similarly to that in the contact mode, that is, by plotting the Z movement of the piezo as a function of the $X–Y$ position. Although the oscillating mode is similar to the contact mode, in that the tip–surface interaction is maintained constant during an AFM scan, the oscillating mode generates smaller lateral forces on the sample, which improves the lateral resolution of the AFM image. Consequently, the oscillating mode is preferred over the contact mode for most biological applications [27].

2.2. Substrates for sample preparation

Flatness and biocompatibility are two basic requirements for substrates used to maintain the integrity of the samples on the surface for imaging. Glass, mica, gold, and silicon surfaces have been used to noncovalently or covalently immobilize biomolecules [28]. The most commonly used substrate is muscovite mica because an atomically flat and negatively charged surface is conveniently obtained by peeling the layered mica prior to sample deposition. Divalent cations, such as Mg^{2+} and Ni^{2+} can be used as salt bridges to absorb negatively charged biomolecules such as DNA onto the mica surface [29,30]. Alternatively, chemical modification of the mica surface can be used to reverse the surface charges to extend its application [31]. In addition, lipid bilayers prepared on mica surfaces by the Langmuir–Blodgett technique can be used as substrates for the reconstitution of membrane proteins [32]. Finally, cationic lipid bilayers on mica have also been used to strongly anchor dsDNA to achieve high-resolution images in liquids [33].

2.3. Imaging in air

In general, imaging in air is much easier than imaging under solution and can provide valuable information about the structural properties of protein–protein and protein–nucleic acid complexes. For imaging in air, the sample is first deposited onto the surface in the desired buffer, which should be filtered using 0.02-μm filters (Fig. 2). For DNA, a reasonable coverage on a mica surface can be obtained with DNA concentrations in the range of 1–10 μg/ml. However, DNA deposition can be dramatically affected by the buffer contents. For example, Mg^{2+} in the buffer can increase DNA deposition onto the mica but monovalent ions will decrease the DNA coverage. For proteins, the required concentration (typically <50 nM) varies depending on the protein and is less dependent on the salt concentration compared to DNA. After deposition of the sample, the surface is rinsed with distilled, dionized water and dried with a gentle stream of nitrogen. Variation in deposition

Stock biological samples (4, -20, -80ºC)

⬇

Dilute/mix samples with buffer

⬇

Make fresh peeled mica

⬇

Incubate sample on the mica

⬇

Wash the mica using H_2O; dry by N_2
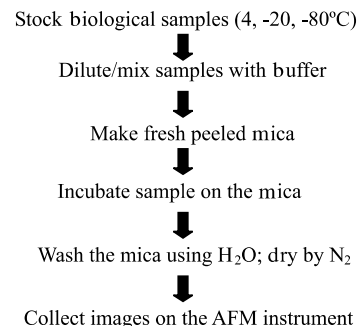
⬇

Collect images on the AFM instrument

Fig. 2. General procedure for AFM imaging in air.

procedures can affect the quality of the deposition. For example, longer incubation on the surface can increase coverage of molecules but it also increases the chances that the molecules or complexes are altered by interaction with the surface. The shortest incubation time that gives reasonable coverage is optimal. Rinsing the surface is required to remove buffer components, but over-washing could denature samples and decrease the coverage. Underdrying can reduce AFM resolution because macromolecules can move around on the moist surfaces. Conversely, overdrying could destabilize some proteins because of dehydration of the protein.

2.4. Imaging in liquid

There are many attractive features with regard to operating an AFM in liquids. The most obvious one is the ability to follow the dynamic structural changes of native single molecules and the interactions between macromolecules in physiologically relevant buffers in real time. For imaging in liquids, a liquid chamber is needed to seal the buffer and allow for buffer exchange. The setup of a standard liquid chamber is shown in Fig. 3. A flow apparatus can be set up to facilitate the switching between different buffers and to minimize the thermal drift of the instrument [34]. Accessory proteins, substrates, cofactors and/or inhibitors can be injected into the fluid chamber. These procedures permit one to observe dynamic conformational changes of the same single protein or the interactions between macromolecules before and after the addition of these chemical and physical factors [35,36]. Accordingly, direct correlation between structural and functional states of individual biomolecules can be made. Such information can be elusive using other techniques such as electron microscopy, crystallography, and AFM in air, which take static pictures of macromolecules in nonnative environments. The second major advantage of imaging in liquids is the minimal force that can be applied to the

sample during imaging due to the elimination of capillary forces [37]. Consequently, the deformation of biological samples is reduced relative to imaging in air, which is a prerequisite to high-resolution imaging of soft biological samples. High-resolution imaging in liquids will be discussed in more detail in Section 4 in this review. Finally, imaging in liquids is advantageous because artifacts related to washing and drying of the samples can be eliminated [38,39].

For close-packed macromolecules, such as two-dimensional (2D) crystal arrays, the contact mode in liquids has generated subnanometer resolution images [32,40,41], but the oscillating mode in liquids is generally preferable over the contact mode for imaging samples with macromolecules loosely attached to the surface. The oscillating mode minimizes lateral forces exerted by the tip and the detachment of the sample from the surface during the scan. Amplitude imaging in the oscillating mode is the most commonly used technique, but it has been shown that, in some cases, mobile DNA in liquids can be more clearly resolved using phase imaging rather than amplitude imaging [42]. Phase imaging in the oscillating mode can broaden the range of conditions for AFM imaging in liquids and can increase the amount of information obtained.

So far, only a small percentage of the published work done using AFM has been performed in liquids because imaging biomolecules in aqueous solutions remains a challenge. First, to watch the dynamic processes in liquids, the right conditions must be identified. Specifically, the samples must bind tightly enough to the surface to allow good imaging but loosely enough to allow the interactions to occur on the surface [34,43]. Second, conventional liquid imaging techniques achieve quality images less than 50% of the time. Finally, the scan rates of commercial AFMs are slow. Many biological reactions happen on the order of milliseconds to seconds, but for commercial AFMs, it will take about 30 s to collect a 1×1-µm image at a reasonable resolution [43].
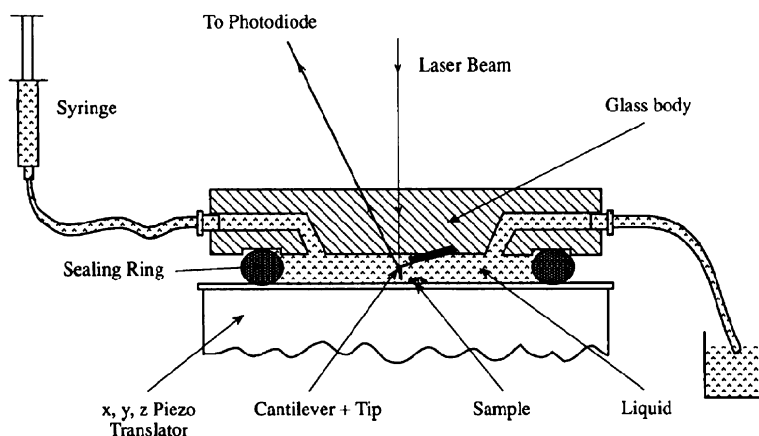

Fig. 3. Cross-section of standard AFM liquid cell. Reproduced from [95].

In the past several years, however, developments in the instrumentation and the probes to increase the reliability of the instrument and the scan rate have been made. These developments will be further discussed in Section 4 in this review.

2.5. Postprocessing of AFM images and generating of quantitative data

The first step after collecting AFM images is postprocessing of images. For example, surface flattening is important for quantitative analyses of AFM images. The software controlling AFM instruments, such as the Nanoscopes of Digital Instruments (Santa Barbara, CA), can accomplish this task using planefit. Additional programs, such as Image SXM (http://reg.ssci.liv.ac.uk/) and NIH Image, are useful for quantitative analysis of the size and shape of molecules and complexes.

3. Quantification of biomolecular assemblies and interactions using AFM

3.1. Characterization of DNA–protein assemblies

The intracellular regulation of gene metabolism involves many proteins, which can bind to regulatory sites on DNA specifically and to other sites nonspecifically. Searching for target sites among the vast amount of nonspecific sites by these proteins is critical for gene regulation [44,45]. Large conformational changes in both proteins and DNA can occur when proteins bind to DNA or exchange between specific sites and nonspecific sites.

Using AFM to investigate the conformations of DNA–protein assemblies is straightforward because the topographic difference between proteins and DNA is obvious in an AFM image. Conformations of DNA–protein assemblies can be quantitatively distinguished by the DNA bend angle induced by protein binding. Two early AFM studies demonstrated the DNA bending ability of *Escherichia coli* RNA polymerase (RNAP) [46] and bacteriophage λ Cro, a small transcription regulatory protein [45] (Fig. 4). The different bent conformations of DNA induced by RNAP were proposed to be the characteristics of polymerase transiting from the open promoter complexes to the elongation complexes [46]. In the Cro study, Erie et al. [45] analyzed the fundamental roles of protein-induced DNA bending at specific sites and at nonspecific sites. Protein-induced bending at nonspecific sites may be important for protein in searching for specific sites and increasing specificity on the target sites [45]. DNA bending induced by many other DNA binding proteins has been observed by AFM [47–49]. Whereas other DNA bending assays, such as gel mobility and X-ray crystallography, yield a single or average bend angle, AFM provides the spatial distribution of bending along the DNA and dynamic
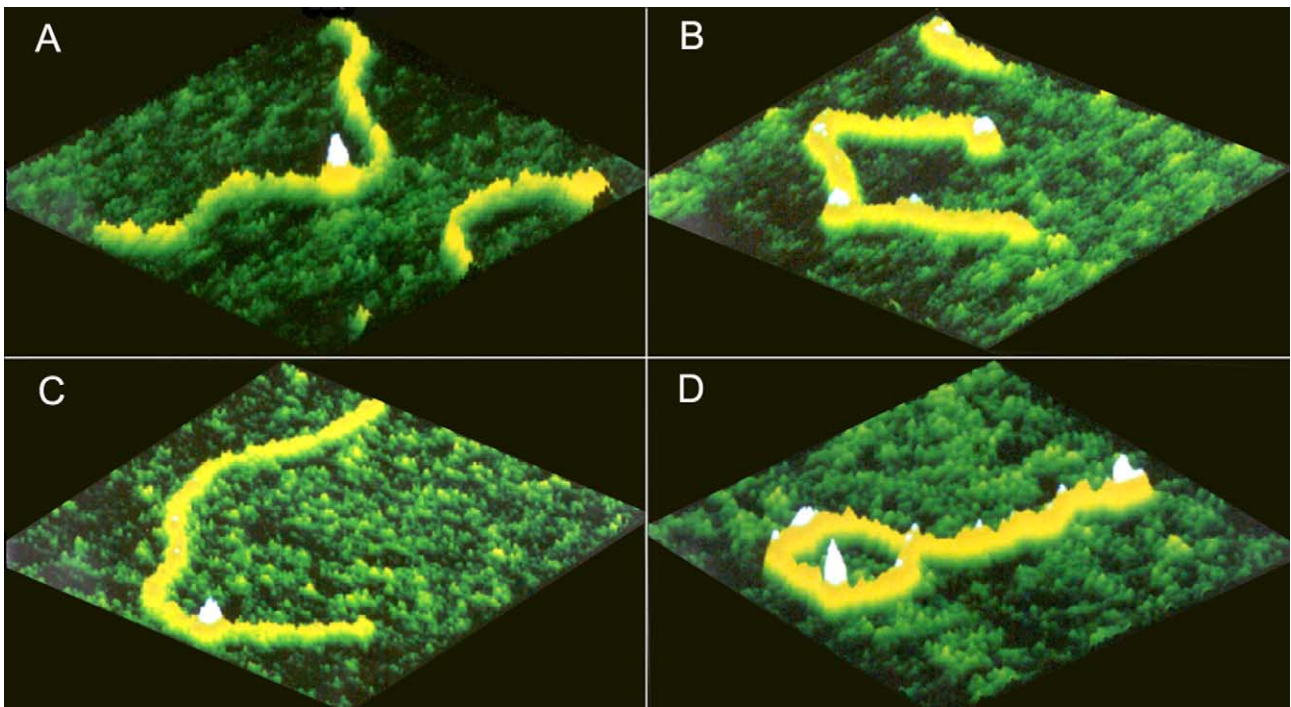

Fig. 4. DNA bending induced by Cro bound at specific sites (A, B) and at nonspecific sites (C, D). The DNA is a 1-kb double-strand fragment containing the λ O_R region to which Cro binds located between 370 and 440 bp from one end of the DNA. The scan sizes are 250 nm. The images are the same as those in [45].

bending histograms of DNA–protein assemblies bound at the same location; that is, the full distribution of angles is observed.

In addition to DNA bending, other quantitative information can be obtained using AFM topographic analysis. For example, a reduced DNA contour length induced by the binding of *E. coli* RNAP holoenzyme has been observed using AFM. This result led to the proposal that DNA wraps around RNAP in the open promoter complex [50]. Other examples include the characterization of the sequence specificity of S1 and mung bean endonucleases by analyzing the distribution of the lengths of the digested DNA [51] and monitoring the change in the specificity of *trp* repressor with the change of enzyme concentrations [52]. Finally, AFM topographic analysis can be used in a qualitative way combined with quantitative assays. For example, the ATP-stimulated unwinding activity of *E. coli* DbpA, a RNA helicase, has been observed using AFM in air [9]. The DNA loop structure induced by the association of *E. coli* RNAP and nitrogen regulatory protein C (NtrC) on DNA also has been characterized using AFM in air [53].

3.2. Determination of the stoichiometries of biomolecular assemblies using volume analysis

3.2.1. Protein–protein assemblies

The intracellular functions of gene regulators are normally implemented by protein oligomers or multiprotein assemblies rather than single proteins. Determining the stoichiometry of these assemblies and the thermodynamics governing their formation are essential to understanding the gene regulation.

Although the heights of proteins as measured by AFM can be affected by various factors, such as the orientation of proteins on the surface and electrostatic interactions between macromolecules and the tip [54], the volumes of proteins in AFM are consistent. It has been shown using a large number of proteins that there is a quantitative linear dependence of the AFM volume on the molecular mass of proteins [55–59] (Fig. 5). Consequently, volume analysis is a robust and reliable method to obtain the stoichiometries of protein–protein assemblies [58,60]. In addition, this volume analysis can be used to determine protein–protein association constants. Recently, it has been used to determine the association constant for the dimerization of *E. coli* DNA helicase II, UvrD, in which the shifts in the distribution of protein oligomeric states under different protein concentrations were analyzed [60]. This study demonstrated the capability of AFM to directly measure thermodynamic properties by comparing their result to the study using analytical ultracentrifugation [60]. AFM volume analysis is useful because it can compensate for the limitations of other techniques. For example, analytical ultracentrifugation and isothermal titration cal-
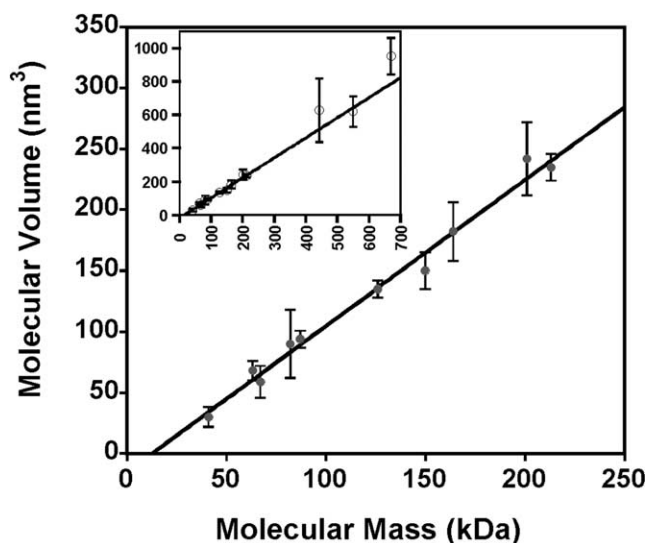

Fig. 5. Plot of protein volume versus molecular mass. The volumes were determined as described in reference [60]. Data are shown for 13 proteins and protein–protein complexes. In the main plot, there are alcohol dehydrogenase (41 kDa), hWRN-N$_{70-240}$ trimer (63 kDa), bovine serum albumin (67 kDa), UvrD monomer (82 kDa), PCNA trimer (87 kDa), hWRN-N$_{70-240}$ hexamer (126 kDa), hWRN-N$_{70-240}$ trimer and PCNA trimer complex (150 kDa), UvrD dimer (164 kDa), β-amylose (201 kDa), hWRN-N$_{70-240}$ hexamer, and PCNA trimer complex (213 kDa). The inset plot also includes apoferritin (443 kDa), RNA polymerase (550 kDa), and thyroglobulin (670 kDa). The line represents the weighted least-square fit of the data, which is described by the following equation: $V = 1.2 (MW) - 14.7$, where V is AFM volume and MW is molecular weight ($R^2 = 0.986$). The error bars represent the standard deviation of the distribution for each protein. The data are taken from references [59–60] and unpublished results.

orimetry require high concentrations of samples, which would limit their use in assaying proteins with low solubility or with tight binding constants.

While volume analysis is a powerful method for determining protein stoichiometries and protein association constants, care must be taken when acquiring the images [60]. First, the tip geometry and the strength of tip–surface interaction need to be consistent in all the experiments, because AFM images are the convolution of tip–surface interactions. Otherwise, a well-defined standard is required in the calibration of different experiments. In addition, the use of volume analysis is not easily applicable to the proteins less than 20 kDa because of the limitation of AFM resolution.

3.2.2. Multiprotein assemblies on the DNA

AFM volume analysis is also useful for determining the oligomeric state of proteins in large DNA–protein assemblies. For example, the oligomeric state of the N-terminal, a fragment of the human WRN gene product has been studied using AFM volume analysis [59]. The study showed that hWRN-N-terminal fragment is in a trimer–hexamer equilibrium in the absence of DNA, but it is primarily a hexamer, the active form for its

functions, in the presence of DNA substrates. In another example, the effects of phosphorylation and mutation of NtrC from *Salmonella typhimurium* on their oligomeric states at specific DNA sites have been studied using volume analysis. This study provided evidence that large oligomers of NtrC are important for activating transcription [61]. Recently, the cooperative binding of Mlh1–Pms1 heterodimer, a DNA mismatch repair protein in yeast, on the DNA has been observed using

AFM [62] (Fig. 6). Although it is difficult to accurately quantify the number of proteins in long tracts of protein assemblies on the DNA with volume analysis, the number of proteins can be estimated from the DNA length covered by proteins, which can be compared to the result from DNA footprinting studies. For example, the oligomeric states of PapB protein, an upstream transcriptional regulator of the pap genes in *E. coli*, have been estimated using this method [63].
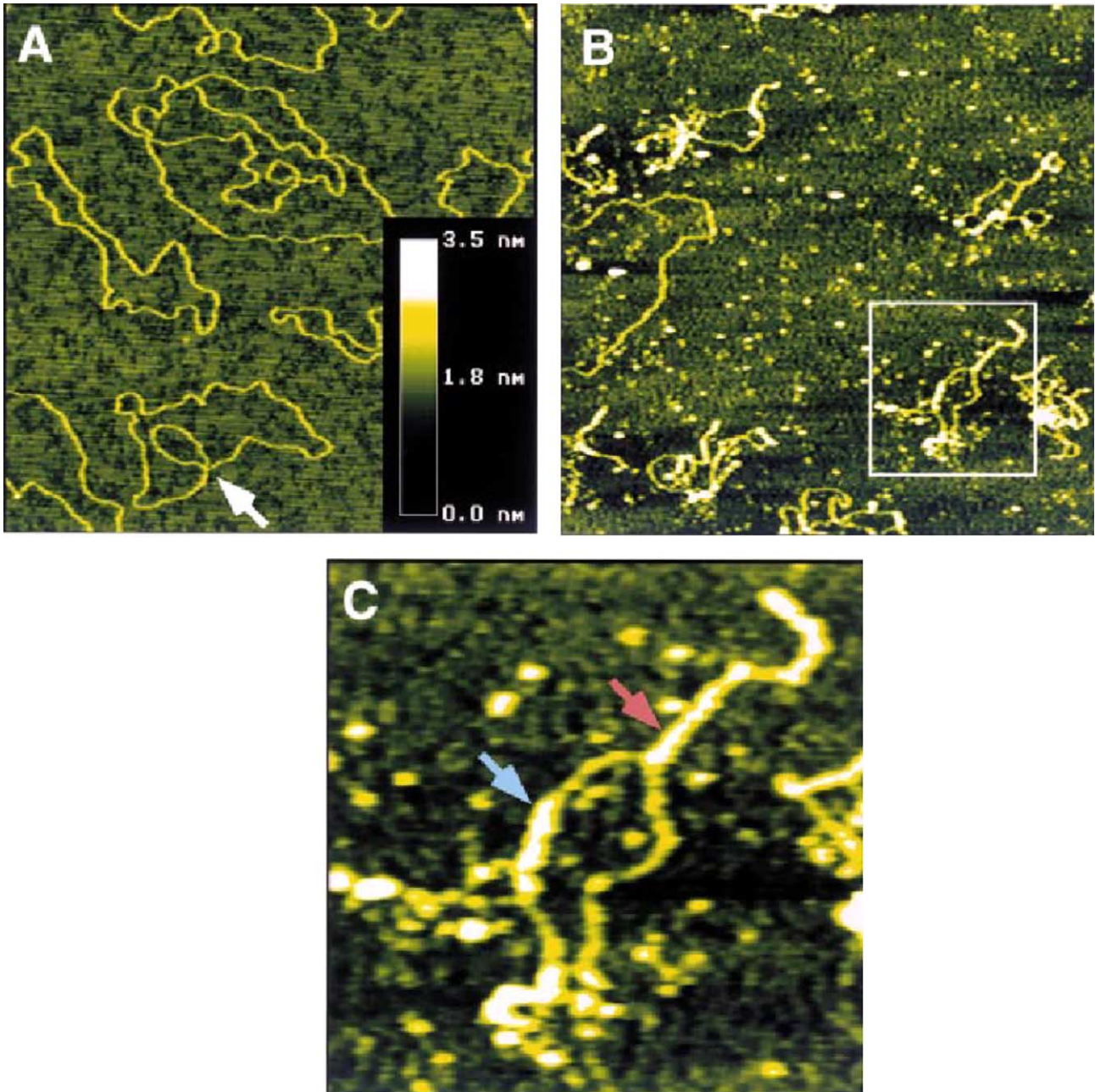

Fig. 6. Cooperative binding of yeast Mlh1–Pms1 heterodimer to dsDNA. (A) M13mp2 RF1 DNA alone. (B) M13 RF1 DNA in the presence of Mlh1–Pms1. The scan sizes are 1500 nm for (A) and (B). (C) Zoomed view of the boxed region in (B). The light gray arrow indicates a tract of cooperatively bound Mlh1–Pms1 associated with a single dsDNA region. The dark gray arrow indicates a tract of cooperatively bound Mlh1–Pms1 associated with two dsDNA regions. Reproduced from [62].

3.3. Following the biological processes using solution imaging

The biomolecular assemblies and interactions in biological pathways take place in a timed fashion in the cell. Time-lapse AFM in solution can be used to follow these processes under near-physiological conditions. For example, the DNA-directed synthesis of RNA by *E. coli* RNAP has been observed using AFM solution imaging [42]. In addition, the degradation of DNA by the nuclease DNase I was followed by oscillating mode AFM in solution in the presence of nickel ions [64]. Many quantitative dynamic properties of these processes can be obtained using time-lapse AFM in solution. For example, the rate of the diffusion of *E. coli* RNAP on DNA was measured using time-lapse AFM. The rate was found to be 1.5 nucleotide/s, which is about 3 times slower than the speed in solution, as expected because the surface hampers the translocation [34]. In another example, the turnover lifetime of GroEL–GroES complexes, a chaperonin/cochaperonin complex, was measured using fast speed 1D AFM in solution [65]. The 1D AFM imaging can be 512 times faster than the conversional 2D AFM imaging because 1D imaging takes only the measurements on one line of the surface but 2D imaging takes the measurements on 512 lines of the surface. In 1D AFM images, one axis is the position on the line; another axis is the time of measurements; the other axis is the height similar to conversional 2D AFM (Fig. 7). This study showed that GroES can accomplish one round of binding to and subsequently dissociating from GroEL in 2 s in the presence of ATP. Finally, very detailed enzyme kinetics of phospholipase A_2 has been analyzed using AFM imaging [15].

In addition to the above quantitative assays, it is also possible to qualitatively but directly correlate structural conformations and functional states of individual biomolecular assemblies using real-time AFM [66]. For example, the conformational change of nuclear pore complexes modulated by ATP, calcium, and carbon dioxide have been studied using time-lapse AFM [67–69]. These studies disclosed that ATP and calcium induce pore contraction and facilitate the transportation of macromolecules between the nucleolus and the cytosol, but carbon dioxide induces pore collapse and functions to isolate the nucleus. Although time-lapse AFM has powerful capabilities, limitations on this dynamic approach also exist. First, the resolution
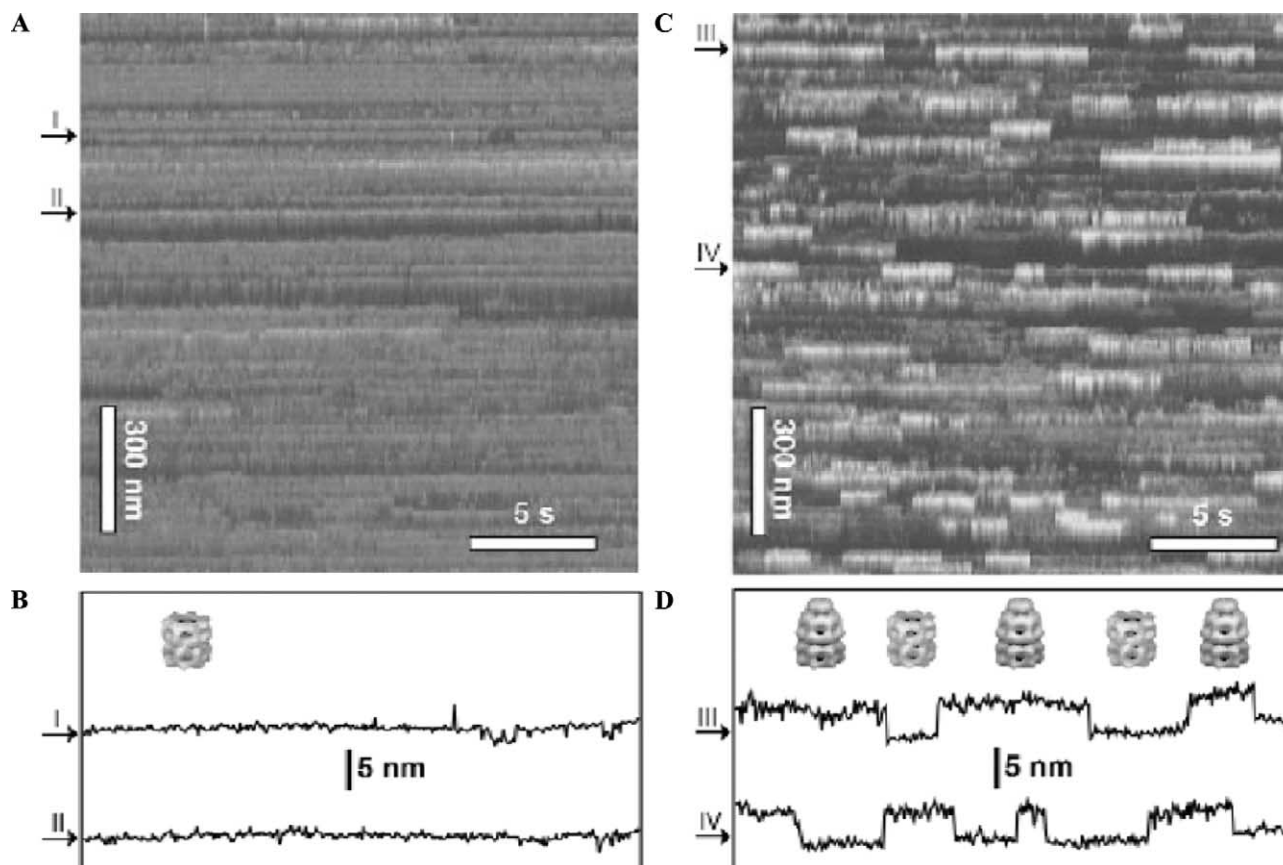

Fig. 7. Association and dissociation processes of GroEL–GroES complexes. (A) 1D AFM image of GroEL in the absence of GroES. (B) Real-time plot of the height of two GroEL molecules monitored in (A). (C) 1D AFM image of GroEL in the presence of GroES (144 nM) and Mg–ATP (2.5 mM). (D) Real-time plot of the height of two GroEL molecules monitored in (C). The images are reproduced from [65].

limitation due to the noise in time-lapse solution imaging limits its use in small biomolecular assemblies. Second, the limitation of scanning speed of commercial AFM instruments cannot accommodate many fast biological processes [70]; however, this limitation is being overcome with recent instrumentation (see Section 4).

3.4. Measurement of forces of interactions between biomolecules

The ability to form biomolecular assemblies is fundamentally governed by the long-range and short-range interacting forces between macromolecules. Thermodynamics and dynamics are the traditional tools for determining the strength of biomolecular interactions. Although the force between interacting components can be measured directly by some methods, such as the surface force apparatus, they lack the spatial resolution to give information at the molecular level [71]. Recent developments on force mode AFM and optical tweezers opened an exciting area for understanding the strength of interactions at a single-molecule level [72]. Further-

more, the tip size with a radius of curvature in the nanometer range enables us to gain spatially resolved force maps over macromolecular surfaces [73]. With regard to sensitivity of force measurements, conventional AFM can detect forces in the range of 0.01–100 nN [74]. Moreover, subpiconewton forces can be resolved utilizing current instrumental developments [75]. This detection limit would meet the requirements needed for the interacting forces in biomolecular assemblies, which are in the piconewton range [71,76].

In the force mode AFM, the interaction between AFM tips and surfaces is recorded as force curves when tips approach or retract from surfaces [6]. The absolute force can be deduced from the spring constant of cantilevers using established force laws (see [73] for review). The components for the force measurement are illustrated in Fig. 8. In a force measurement, one interacting partner is attached to the AFM tip using techniques such as chemical coating and biological functionalizations [77]. Similar techniques have been used to immobilize other interacting partners on the surface [78], which can improve the reproducibility of force mea-
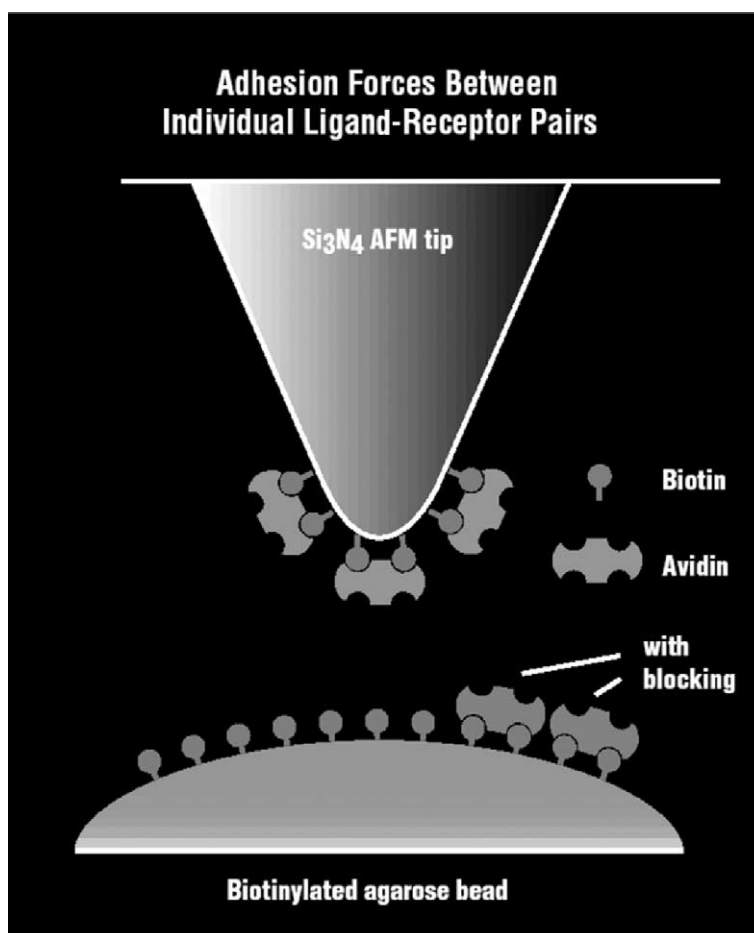

Fig. 8. Schematic view of force measurements. One partner (avidin) in biomolecular interactions is attached on the AFM tips. Another partner (biotin) is immobilized on the surface. Reproduced from [71].

surements [20]. Force microscopy has been applied in many biological areas, such as antigen–antibody pairs, protein–ligand interactions, protein–membrane interactions, and protein–cell interactions. A detailed review of these applications is out of the range of this article and some excellent reviews are available elsewhere [74,76,79].

Although force microscopy has powerful capabilities, some limitations in current force microscopy applied in biological investigations exist. The force measurements are so sensitive to the sample preparation and the conditions of measurements that it is difficult to compare the absolute forces obtained by different research groups. Consequently, monitoring the force changing with conditions, such as the conditions of the measurement and the buffer, is a more reliable way to understand molecular interactions in cell biology than measuring absolute force values. Additionally, there are no universal approaches that can be used for preparing various biological samples, which could limit its use in some biological systems.

4. Recent developments in biological AFM

4.1. High-resolution imaging

Since the invention of AFM, many developments to increase its resolution have been made. It is well established now that in addition to instrumental factors, major factors that can affect the quality of the image include shape of the tip tip–sample interactions, stable immobilization of the sample on the surface, and both pH and ionic strength of the buffer used for absorbing and scanning the sample [33,54,80,81]. At room temperature, easy deformation by the scanning tips and thermal motion of most macromolecules make it hard to achieve high-resolution images. Close packing of the sample on the surface can reduce this problem to some degree and achieve subnanometer resolution under solution [32,40,41], but cryo–AFM holds the promise for imaging a large variety of biological samples at high resolution comparable to EM [82,83]. Meanwhile, even with state-of-art techniques such as cryo–AFM, the resolving power of AFM will not be fully reached without a well-defined ultrasharp tip. Carbon nanotube probes are the most promising candidates for the next generation of ultrasharp AFM probes [81,84].

4.1.1. 2D crystals
Due to limited hydrophilic surfaces, membrane proteins do not readily form 3D crystals for X-ray crystallography, but 2D membrane protein crystals reconstituted in the presence of lipids are more stable and a large number of membrane proteins have been crystallized in this manner. Electron crystallography of 2D crystals has provided static structural information at

atomic resolution [32]. Imaging in liquids using AFM provides an advantage over EM, in that the native environments and biological activities of these membrane proteins can be preserved throughout sample preparation and scanning. AFM is the only technique that gives insights into both the surface structures and dynamics of membrane proteins at subnanometer resolution. The high resolution is partly due to the elimination of capillary forces [37]. Müller et al. [80] demonstrated that by adjusting the pH and electrolytes in the buffer, electrostatic double-layer repulsion between the tip and the sample can be reduced, resulting in reduced vertical and lateral forces between the AFM tip and the sample. In addition, the 2D crystals are strongly anchored to the substrates in liquids, and the force applied to the AFM tips is believed to be distributed over a large sample area on these 2D crystals. The factors mentioned above collectively dramatically reduce the sample deformation during scanning. In addition, only the small sharp protrusion at the end of tip is believed to sense the short-range electrostatic repulsion that confers high-resolution structural information. The subnanometer resolution imaging is demonstrated by the images of purple membrane (which consists of bacteriorhodopsin and lipids) shown in Fig. 9 [80]. A lateral resolution of 0.6 nm (width at half-maximum height) is reproducible in these images.

4.1.2. Cryo–AFM
It has been shown that the mechanical rigidity of biological materials is significantly stronger at cryogenic temperatures. The estimated Young's modulus of protein and DNA is between 10^3 and 10^4 times of that at room temperature [83], dramatically reducing the deformation by the scanning tip. With decreased thermal motion and increased rigidity of the samples, high-resolution 3D images were demonstrated by cryo–AFM [83,85]. Some images from cryo–AFM also revealed information that was not obvious in electron micrographs. For example, cryo–AFM showed a protrusion in the center of IgM protein, which was not obvious in previous EM images [83]. For structural studies of large flexible complexes, cryo–AFM will be a very effective alternative, capable of providing information that could be elusive to other techniques.

4.1.3. Carbon nanotube probes
As mentioned before, AFM probes are essential to high-resolution, reproducible imaging of biological samples. The widely used microfabricated Si and Si_3N_4 AFM probes have several disadvantages, such as large radii of curvature compared to the biological sample size and brittleness. The high-resolution imaging of membrane proteins achieved using microfabricated probes was attributed to the small protrusions at the end of the tips. These small protrusions are not consistent from probe to probe. Carbon nanotubes consists of seamless
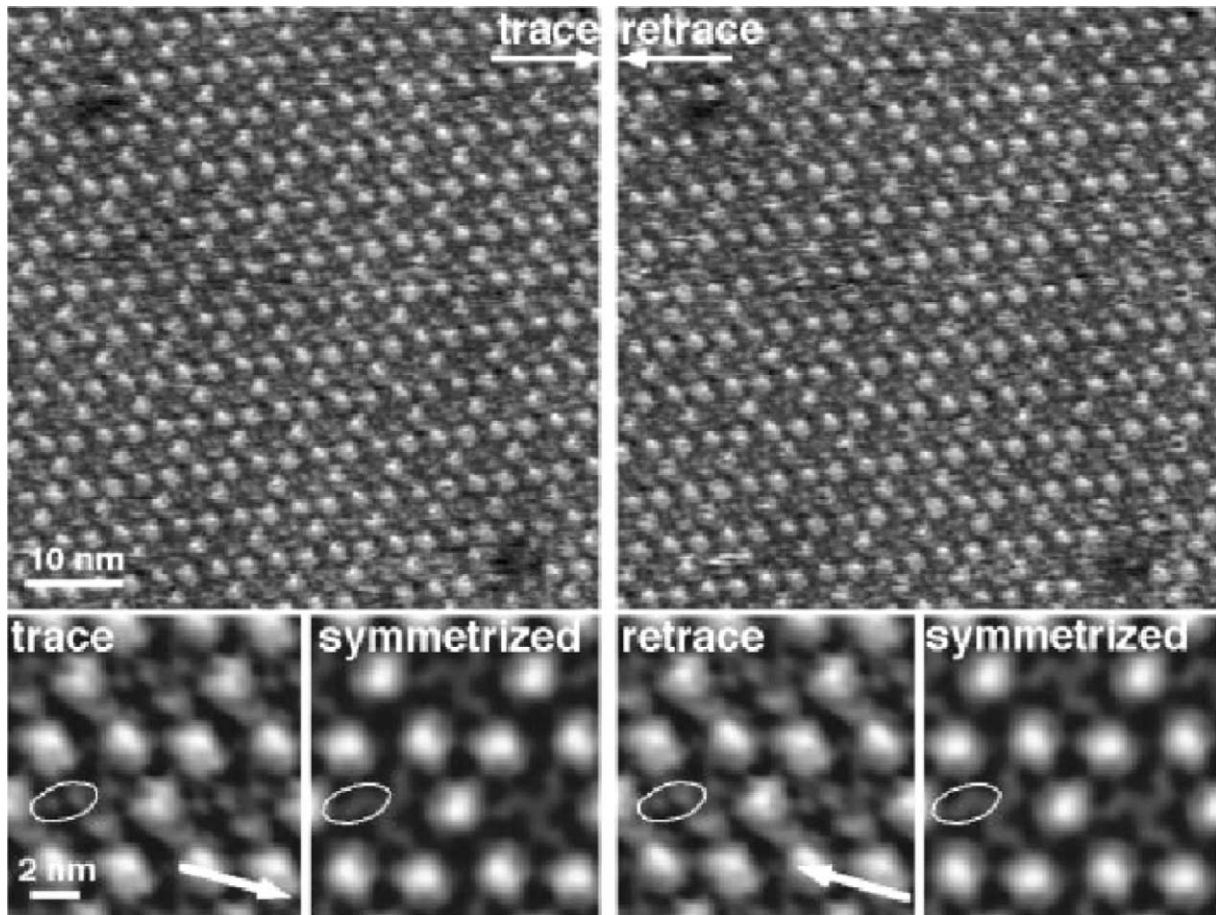
Fig. 9. High-resolution images of extracellular surface of reconstituted 2D purple membrane protein. Structural details are identical in the trace and retrace directions, demonstrating minimized deformation. Three main domains make up a horseshoe-like structure in each bacteriorhodopsin trimer. The ellipse indicates the smallest details resolved, which have a width at half-maximum height of 0.6 nm. The images were collected at applied forces of 0.1 nN. Reproduced from [80].

cylinders made from sp^2-bonded carbon. The small radii (0.7–5 nm for single-walled nanotubes), high aspect ratio, extremely large Young's modulus (stiffness), and ability to be elastically buckled under large load make carbon nanotubes ideal candidates for use as AFM probes. The past several years have seen the development of the technologies to directly grow carbon nanotubes onto the pyramids of microfabricated tips to overcome the low efficiency of manual assembly. There are several elegant review papers on the fabrication technologies and high-resolution imaging using carbon nanotubes [81,84,86]. Using carbon nanotube probes, Umemura et al. [87] have observed the 10-nm pitch of RecA–dsDNA complexes, which was consistent with measurement on electron micrographs. This result demonstrated the increase of resolution using carbon nanotubes. Before, using the standard microfabricated probes, the pitch was observed as 20–30 nm. Another common problem encountered with microfabricated AFM probes is that they are easily contaminated by the biological samples during scanning. In regard to this problem, the promise of carbon nanotubes as AFM probes is waiting to be tested on a wide range of samples.

4.2. Magnetic mode (MAC) and photothermal mode (PMOD) AFM for imaging in liquids

As mentioned before, conventional liquid imaging techniques are not reliable. An intrinsic problem in the instrument is that a piezoelectric transducer vibrates the AFM probe indirectly by oscillating the probe holder. This leads to the masking of the resonance peak of the cantilever by the vibrations from the probe holder and the fluid body. In the past several years, MAC and PMOD have been used to directly vibrate the cantilever and increase the reliability of imaging in liquids [88,89]. MAC uses a cantilever that has a magnetic particle attached to it or that has magnetic coating, and the cantilever is driven directly by a magnetic field. In PMOD, a bimetallic cantilever is oscillated by a pulsed diode laser. Due to the difference in the thermal expansion coefficients of the two layers, the cantilever bends and vibrates in response to the pulsed laser. Both MAC and

PMOD have demonstrated high-resolution imaging capability on biological samples [88,89]. With the recent commercialization of MAC accessories to standard AFM instruments, imaging in liquids will become more routine in the near future.

4.3. Smaller cantilever and high-speed scanning in liquids

Presently, commercial probes have cantilevers with lengths on the order of 100 μm. Theoretically, deceasing the dimension of the cantilever will have the advantages of lower noise and a higher resonance frequency and will allow for faster scanning. In addition, a smaller cantilever can measure smaller forces due to a lower viscous damping coefficient [55,90]. Hansma's [55] and Hoh's [91] groups pioneered the work to fabricate smaller cantilevers. Recently, a research group in Japan devel-

oped an instrument that in combination with a small cantilever (resonance frequency of 450–465 kHz in water) can capture a 100×100 pixel image (240 nm scan size) in 80 ms. Successive images of the movement of myosin V on mica can be seen at *http://www.s.kanazawa-u.ac.jp/phys/biophys/bmv_movie.htm* [70]. This group predicted an upper limit of 10–20 ms for scanning a 240-nm-size image for their novel design. Commercialization of these techniques in the near future will greatly expand the number of biological systems that can be studied in real time under liquids.

4.4. Single-molecule manipulation with the nanomanipulator

The nanoManipulator system, which was developed at University of North Carolina at Chapel Hill,
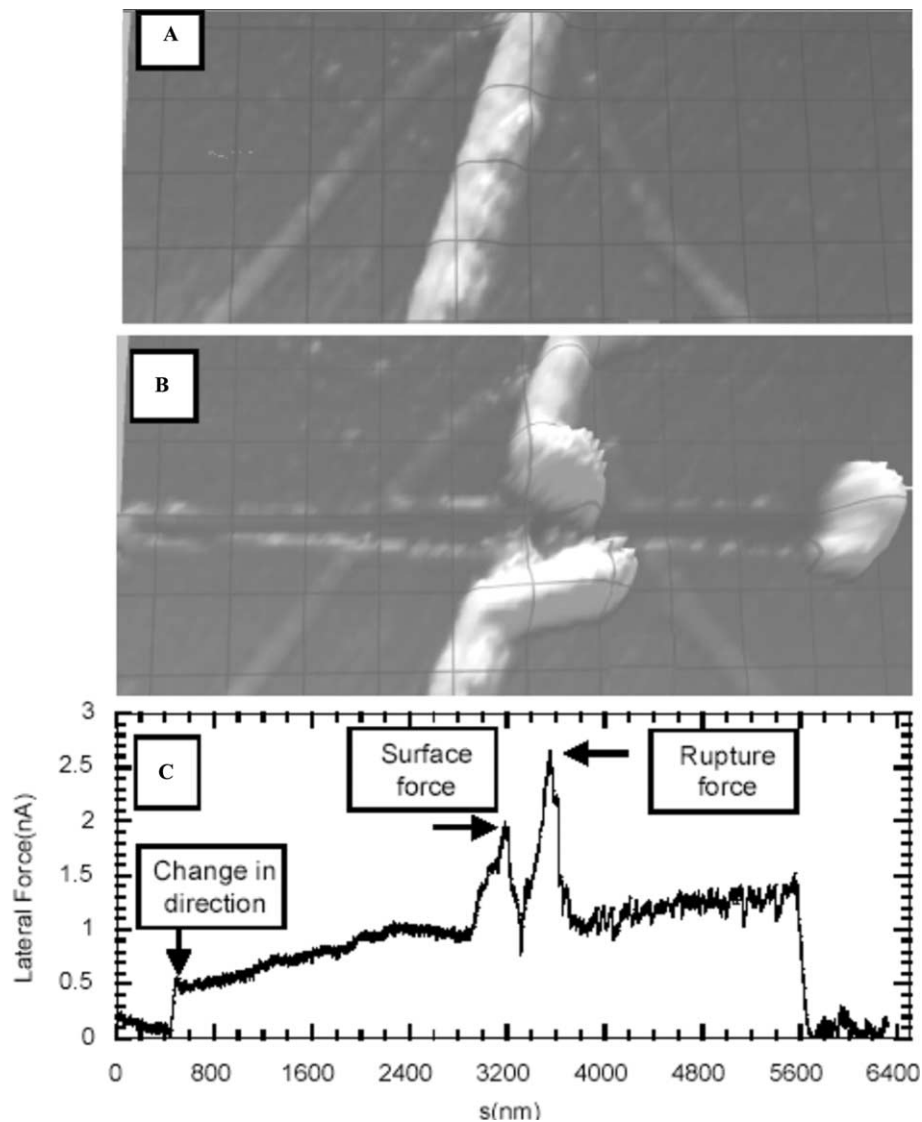

Fig. 10. Manipulation of fibrin using the nanoManipulator. Fibrin fiber (diameter: 150 nm) before (A) and after (B) manipulation. (C) Lateral force trace for manipulation of fibrin fiber. Reproduced from [92].

integrates the AFM with a virtual reality interface that gives investigators new ways of interacting with objects at the nanometer scale [92–94]. Using a force-feedback pen, the user can touch the surface and directly manipulate the object. The manipulation is accomplished by exporting the data to a PHANTOM controller (SensAble Technologies, Cambridge, MA). This procedure allows investigators to precisely locate objects and features by feeling the surface. Samples can be manipulated in the contact mode and the change before and after manipulation can be monitored using oscillating mode imaging. Samples can be bent, translated, rotated, and dissected. Mechanical properties of biological samples can be measured directly by recording the normal and lateral forces during the manipulation process. The rupture forces of fibrin (Fig. 10) and DNA have been measured using the nanoManipulator, and nonspecific binding between adenovirus and surfaces have been monitored [92]. Forces ranging from a few piconewtons to several micronewtons can be measured using the nanoManipulator, expanding the range of forces (10^{-9}–10^{-14} N) measured by other single-molecule manipulation techniques, such as microneedles, flow field, magnetic field, and optical tweezers [72]. Compared to other single-molecule manipulation techniques, the nanoManipulator has the advantages of easy sample preparation and the ability to monitor the sample before and after the manipulation. One disadvantage of this technique is that the surface interaction may complicate the interpretation of the data. In addition to measuring the physical properties of biological samples, in the future, the nanoManipulator may be used as a tool to push the macromolecules together and watch the interaction in real time in liquid.

Acknowledgments

References

[1] G. Binnig, C.F. Quate, C. Gerber, Phys. Rev. Lett. 56 (1986) 930–933.

[2] P.K. Hansma, V.B. Elings, O. Marti, C.E. Bracker, Science 242 (1988) 209–216.

[3] O. Marti, V. Elings, M. Haugan, C.E. Bracker, J. Schneir, B. Drake, S.A. Gould, J. Gurley, L. Hellemans, K. Shaw, et al., J. Microsc. 152 (Pt. 3) (1988) 803–809.

[4] M. Radmacher, R.W. Tillamnn, M. Fritz, H.E. Gaub, Science 257 (1992) 1900–1905.

[5] A. Engel, D.J. Muller, Nat. Struct. Biol. 7 (2000) 715–718.

[6] J. Zlatanova, S.M. Lindsay, S.H. Leuba, Prog. Biophys. Mol. Biol. 74 (2000) 37–61.

[7] H.G. Hansma, Annu. Rev. Phys. Chem. 52 (2001) 71–92.

[8] W. Fritzsche, L. Takac, E. Henderson, Crit. Rev. Eukaryot. Gene Expr. 7 (1997) 231–240.

[9] A. Henn, O. Medalia, S.P. Shi, M. Steinberg, F. Franceschi, I. Sagi, Proc. Natl. Acad. Sci. USA 98 (2001) 5007–5012.

[10] M. Bonin, J. Oberstrass, N. Lukacs, K. Ewert, E. Oesterschulze, R. Kassing, W. Nellen, RNA 6 (2000) 563–570.

[11] J. Liphardt, B. Onoa, S.B. Smith, I.J.R Tinoco, C. Bustamante, Science 292 (2001) 733–737.

[12] Y.L. Lyubchenko, B.L. Jacobs, S.M. Lindsay, Nucleic Acids Res. 20 (1992) 3983–3986.

[13] B. Isralewitz, M. Gao, K. Schulten, Curr. Opin. Struct. Biol. 11 (2001) 224–230.

[14] J.B. Heymann, D.J. Muller, K. Mitsuoka, A. Engel, Curr. Opin. Struct. Biol. 7 (1997) 543–549.

[15] K. Balashev, T.R. Jensen, K. Kjaer, T. Bjornholm, Biochimie 83 (2001) 387–397.

[16] Y.F. Dufrene, G.U. Lee, Biochim. Biophys. Acta 1509 (2000) 14–41.

[17] W. Dettmann, M. Grandbois, S. Andre, M. Benoit, A.K. Wehle, H. Kaltner, H.J. Gabius, H.E. Gaub, Arch. Biochem. Biophys. 383 (2000) 157–170.

[18] G.N. Misevic, Microsc. Res. Tech. 44 (1999) 304–309.

[19] P.E. Marszalek, H. Li, J.M. Fernandez, Nat. Biotechnol. 19 (2001) 258–262.

[20] O.H. Willemsen, M.M. Snel, A. Cambi, J. Greve, B.G. De Grooth, C.G. Figdor, Biophys. J. 79 (2000) 3267–3281.

[21] Y.L. Lyubchenko, B.L. Jacobs, S.M. Lindsay, A. Stasiak, Scanning Microsc. 9 (1995) 705–724, discussion 724–727.

[22] C.R. Safinya, Curr. Opin. Struct. Biol. 11 (2001) 440–448.

[23] H. Oberleithner, J. Geibel, W. Guggino, R.M. Henderson, M. Hunter, S.W. Schneider, A. Schwab, W. Wang, Wien Klin Wochenschr. 109 (1997) 419–423.

[24] T. Danker, H. Oberleithner, Pflugers Arch. 439 (2000) 671–681.

[25] E. Henderson, Prog. Surf. Sci. 46 (1994) 39–60.

[26] F.M. Ohnesorge, J.K. Horber, W. Haberle, C.P. Czerny, D.P. Smith, G. Binnig, Biophys. J. 73 (1997) 2183–2194.

[27] V.J. Morris, A.R. Kirby, A.P. Gunning, Atomic Force Microscopy for Biologists, Imperial College Press, 1999.

[28] P. Wagner, FEBS Lett. 430 (1998) 112–115.

[29] H.G. Hansma, D.E. Laney, Biophys. J. 70 (1996) 1933–1939.

[30] D.J. Muller, M. Amrein, A. Engel, J. Struct. Biol. 119 (1997) 172–188.

[31] Y.L. Lyubchenko, P.I. Oden, D. Lampner, S.M. Lindsay, K.A. Dunker, Nucleic Acids Res. 21 (1993) 1117–1123.

[32] H. Stahlberg, D. Fotiadis, S. Scheuring, H. Remigy, T. Braun, K. Mitsuoka, Y. Fujiyoshi, A. Engel, FEBS Lett. 504 (2001) 166–172.

[33] J. Mou, D.M. Czajkowsky, Y. Zhang, Z. Shao, FEBS Lett. 371 (1995) 279–282.

[34] M. Guthold, X. Zhu, C. Rivetti, G. Yang, N.H. Thomson, S. Kasas, H.G. Hansma, B. Smith, P.K. Hansma, C. Bustamante, Biophys. J. 77 (1999) 2284–2294.

[35] P.A. Osmulski, M. Gaczynska, J. Biol. Chem. 275 (2000) 13171–13174.

[36] H. Oberleithner, S. Schneider, J.O. Bustamante, Pflugers Arch. 432 (1996) 839–844.

[37] B. Drake, C.B. Prater, A.L. Weisenhorn, S.A. Gould, T.R. Albrecht, C.F. Quate, D.S. Cannell, H.G. Hansma, P.K. Hansma, Science 243 (1989) 1586–1589.

[38] A. Schulz, N. Mucke, J. Langowski, K. Rippe, J. Mol. Biol. 283 (1998) 821–836.

[39] F. Nagami, G. Zuccheri, B. Samori, R. Kuroda, Anal. Biochem. 300 (2002) 170–176.

[40] D.J. Muller, D. Fotiadis, A. Engel, FEBS Lett. 430 (1998) 105–111.

[41] D.J. Muller, N.A. Dencher, T. Meier, P. Dimroth, K. Suda, H. Stahlberg, A. Engel, H. Seelert, U. Matthey, FEBS Lett. 504 (2001) 219–222.

[42] M. Argaman, R. Golan, N.H. Thomson, H.G. Hansma, Nucleic Acids Res. 25 (1997) 4379–4384.

[43] Y. Jiao, D.I. Cherny, G. Heim, T.M. Jovin, T.E. Schaffer, J. Mol. Biol. 314 (2001) 233–243.

[44] O.G. Berg, R.B. Winter, P.H. von Hippel, Biochemistry 20 (1981) 6929–6948.

[45] D.A. Erie, G. Yang, H.C. Schultz, C. Bustamante, Science 266 (1994) 1562–1566.

[46] W.A. Rees, R.W. Keller, J.P. Vesenka, G. Yang, C. Bustamante, Science 260 (1993) 1646–1649.

[47] B.W. Allan, R. Garcia, K. Maegley, J. Mort, D. Wong, W. Lindstrom, J.M. Beechem, N.O. Reich, J. Biol. Chem. 274 (1999) 19269–19275.

[48] J. van Noort, F. Orsini, A. Eker, C. Wyman, B. de Grooth, J. Greve, Nucleic Acids Res. 27 (1999) 3875–3880.

[49] G. Hun Seong, E. Kobatake, K. Miura, A. Nakazawa, M. Aizawa, Biochem. Biophys. Res. Commun. 291 (2002) 361–366.

[50] C. Rivetti, M. Guthold, C. Bustamante, EMBO J. 18 (1999) 4464–4475.

[51] K. Umemura, F. Nagami, T. Okada, R. Kuroda, Nucleic Acids Res. 28 (2000) E39.

[52] E. Margeat, C. Le Grimellec, C.A. Royer, Biophys. J. 75 (1998) 2712–2720.

[53] K. Rippe, M. Guthold, P.H. von Hippel, C. Bustamante, J. Mol. Biol. 270 (1997) 125–138.

[54] D.J. Muller, A. Engel, Biophys. J. 73 (1997) 1633–1644.

[55] M.B. Viani, T.E. Schaffer, A. Chand, M. Rief, H.E. Gaub, P.K. Hansma, J. Appl. Phys. 86 (1999) 2258–2262.

[56] H. Oberleithner, S. Schneider, J. Larmer, R.M. Henderson, Kidney Blood Press. Res. 19 (1996) 142–147.

[57] S. Scheuring, P. Ringler, M. Borgnia, H. Stahlberg, D.J. Muller, P. Agre, A. Engel, EMBO J. 18 (1999) 4981–4987.

[58] S.W. Schneider, J. Larmer, R.M. Henderson, H. Oberleithner, Pflugers Arch. 435 (1998) 362–367.

[59] Y. Xue, G.C. Ratcliff, H. Wang, P.R. Davis-Searles, M.D. Gray, D.A. Erie, M.R. Redinbo, Biochemistry 41 (2002) 2901–2912.

[60] G.C. Ratcliff, D.A. Erie, J. Am. Chem. Soc. 123 (2001) 5632–5635.

[61] C. Wyman, I. Rombel, A.K. North, C. Bustamante, S. Kustu, Science 275 (1997) 1658–1661.

[62] M.C. Hall, H. Wang, D.A. Erie, T.A. Kunkel, J. Mol. Biol. 312 (2001) 637–647.

[63] Y. Xia, K. Forsman, J. Jass, B.E. Uhlin, Mol. Microbiol. 30 (1998) 513–523.

[64] M. Bezanilla, B. Drake, E. Nudler, M. Kashlev, P.K. Hansma, H.G. Hansma, Biophys. J. 67 (1994) 2454–2459.

[65] M.B. Viani, L.I. Pietrasanta, J.B. Thompson, A. Chand, I.C. Gebeshuber, J.H. Kindt, M. Richter, H.G. Hansma, P.K. Hansma, Nat. Struct. Biol. 7 (2000) 644–647.

[66] M. Stolz, D. Stoffler, U. Aebi, C. Goldsbury, J. Struct. Biol. 131 (2000) 171–180.

[67] A. Rakowska, T. Danker, S.W. Schneider, H. Oberleithner, J. Membr. Biol. 163 (1998) 129–136.

[68] D. Stoffler, K.N. Goldie, B. Feja, U. Aebi, J. Mol. Biol. 287 (1999) 741–752.

[69] H. Oberleithner, H. Schillers, M. Wilhelmi, D. Butzke, T. Danker, Pflugers Arch. 439 (2000) 251–255.

[70] T. Ando, N. Kodera, E. Takai, D. Maruyama, K. Saito, A. Toda, Proc. Natl. Acad. Sci. USA 98 (2001) 12468–12472.

[71] E.L. Florin, V.T. Moy, H.E. Gaub, Science 264 (1994) 415–417.

[72] C. Bustamante, J.C. Macosko, G.J. Wuite, Nat. Rev. Mol. Cell Biol. 1 (2000) 130–136.

[73] W.F. Heinz, J.H. Hoh, Trends Biotechnol. 17 (1999) 143–150.

[74] D. Leckband, Annu. Rev. Biophys. Biomol. Struct. 29 (2000) 1–26.

[75] M. Tokunaga, T. Aoki, M. Hiroshima, K. Kitamura, T. Yanagida, Biochem. Biophys. Res. Commun. 231 (1997) 566–569.

[76] P.F. Luckham, K. Smith, Faraday Discuss. (1998) 307–320, discussion 331–343.

[77] R.J. Colton, A. Engel, J.E. Frommer, H.E. Gaub, A.A. Gewirth, R. Guckenberger, J. Rabe, W.M. Heckl, B. Parkinson, Procedures in Scanning Probe Microscopies, Wiley, New York, 1998.

[78] Y.L. Lyubchenko, A.A. Gall, L.S. Shlyakhtenko, R.E. Harrington, B.L. Jacobs, P.I. Oden, S.M. Lindsay, J. Biomol. Struct. Dyn. 10 (1992) 589–606.

[79] H. Clausen-Schaumann, M. Seitz, R. Krautbauer, H.E. Gaub, Curr. Opin. Chem. Biol. 4 (2000) 524–530.

[80] D.J. Muller, D. Fotiadis, S. Scheuring, S.A. Muller, A. Engel, Biophys. J. 76 (1999) 1101–1111.

[81] J.H. Hafner, C.L. Cheung, A.T. Woolley, C.M. Lieber, Prog. Biophys. Mol. Biol. 77 (2001) 73–110.

[82] Z. Shao, D. Shi, A.V. Somlyo, Biophys. J. 78 (2000) 950–958.

[83] Z. Shao, Y. Zhang, Ultramicroscopy 66 (1996) 141–152.

[84] A.T. Woolley, C.L. Cheung, J.H. Hafner, C.M. Lieber, Chem. Biol. 7 (2000) 193–204.

[85] Y. Mat-Arip, K. Garver, C. Chen, S. Sheng, Z. Shao, P. Guo, J. Biol. Chem. 276 (2001) 32575–32584.

[86] R.M.D. Stevens, N.A. Frederick, B.L. Smith, D.E. Morse, G.D. Stucky, P.K. Hansma, Nanotechnology 11 (2000) 1–5.

[87] K. Umemura, J. Komatsu, T. Uchihashi, N. Choi, S. Ikawa, T. Nishinaka, T. Shibata, Y. Nakayama, S. Katsura, A. Mizuno, H. Tokumoto, M. Ishikawa, R. Kuroda, Biochem. Biophys. Res. Commun. 281 (2001) 390–395.

[88] W. Han, S.M. Lindsay, T. Jing, Appl. Phys. Lett. 69 (1996) 4111–4114.

[89] G.C. Ratcliff, D.A. Erie, R. Superfine, Appl. Phys. Lett. 72 (1998) 1911–1913.

[90] M.B. Viani, T.E. Schaffer, G.T. Paloczi, L.I. Pietrasanta, B.L. Smith, J.B. Thompson, M. Richter, M. Rief, H.E. Gaub, K.W. Plaxco, A.N. Cleland, H.G. Hansma, P.K. Hansma, Rev. Sci. Instrum. 70 (1999) 4300–4303.

[91] A.R. Hodges, K.M. Bussmann, J.H. Hoh, Rev. Sci. Instrum. 72 (2001) 3880–3883.

[92] M. Guthold, M. Falvo, W.G. Matthews, S. Paulson, J. Mullin, S. Lord, D. Erie, S. Washburn, R. Superfine, F.P. Brooks, R.M. Taylor, J. Mol. Graphics Modell. 17 (2000) 187–197.

[93] M. Guthold, G. Matthews, A. Negishi, R.M. Taylor, D. Erie, F.P. Brooks Jr., R. Superfine, Surf. Interf. Anal. 27 (1999) 437–443.

[94] M. Sincell, Science 290 (2000) 1530.

[95] M. Guthold, M. Bezanilla, D.A. Erie, B. Jenkins, H.G. Hansma, C. Bustamante, Proc. Natl. Acad. Sci. USA 91 (1994) 12927–12931.